Available online at www.sciencedirect.com

ScienceDirect

Procedia Manufacturing 53 (2021) 427–434

Procedia MANUFACTURING

www.elsevier.com/locate/procedia

49th SME North American Manufacturing Research Conference, NAMRC 49, Ohio, USA

In-situ Droplet Monitoring of Inkjet 3D Printing Process using Image Analysis and Machine Learning Models

Michael Ogunsanya[a], Joan Isichei[a], Santosh Kumar Parupelli[a], Salil Desai[a], Yi Cai[b,*]

[a]*Department of Industrial and Systems Engineering, North Carolina Agricultural and Technical State University, Greensboro, North Carolina, United States*
[b]*Department of Applied Engineering Technology, North Carolina Agricultural and Technical State University, Greensboro, North Carolina, United States*

* Corresponding author. Tel.: +1-336-285-3162; fax: +1-336-334-7704. *E-mail address:* ycai@ncat.edu

Abstract

Additive manufacturing (AM) has yielded major innovations in the electronics, biomedical and energy domains. One of the AM techniques which has witnessed widespread use is the inkjet 3D printing (IJP). The IJP process fabricates parts by depositing colloidal liquid droplets on substrates. Despite its advantages, variations in input process parameters and fluid properties can have a profound impact on the print quality. This paper aims to address this issue by presenting a novel vision-based approach for *in-situ* monitoring of droplet formation. Further, a machine learning model was used to study the relationship between droplet attributes and droplet modes. A drop watcher camera was used to capture a sequence of videos obtained from different combinations of voltage and frequency. Custom source code was developed using python libraries to capture variations in droplet attributes (droplet size, velocity, aspect ratio, and presence of satellites) and their impact on the droplet modes (normal, satellite, and no-droplet) using computer vision. A backpropagation neural network mode (BPNN) was applied, with the droplet features as inputs, to classify output droplet modes. The BPNN classified droplet modes with 90% (high) accuracy. This research forms the basis for future development of digital twin model of inkjet 3D printing towards predictive analysis and process optimization.

Keywords: additive manufacturing; inkjet 3D Printing; image analysis; machine learning; neural network.

1. Introduction

Additive Manufacturing (AM), popularly known as 3D Printing, is the "process of joining materials to make objects from 3D model data usually layer-by-layer, as opposed to subtractive manufacturing technologies such as traditional manufacturing". AM has been hailed as the third industrial revolution which enables the fabrication of complex freeform designs. AM is a creative technology which has the capability to revolutionize the global manufacturing industry [1]. According to American Society for Testing and Materials (ASTM), there are different types of additive manufacturing processes, including photo-polymerization process, extrusion-based systems, powder bed fusion processes, material jetting processes, binder jetting processes, beam deposition processes, sheet lamination processes and direct write technologies [2]. AM has numerous benefits over the traditional and subtractive manufacturing methods. Some of the important benefits include complexity, efficiency, flexibility, high degree of design freedom, reduced assembly and predictable production [3]. The materials that can be used for fabricating 3D structures include metallic, polymers, ceramics, and composites. Initially, AM known as rapid prototyping was developed for building prototypes only, With the advancement of the technologies and materials AM has broadened its applications into a wide range of fields such as biomedical, aerospace, electronics, automobile, construction, food industry, consumer, jewelry, military, and manufacturing [4-9].

Inkjet 3D printing (IJP) [10] is one of the most popular AM techniques that deposits a sequence of sub-millimeter (micro scale) liquid droplets with very high precision and accuracy. The deposition can be customized to build both 2D and 3D

2351-9789
10.1016/j.promfg.2021.06.045

printed artifacts. Of all the AM processes, inkjet printing has emerged at the frontline due to the following desirable features: low cost, high pattern precision and resolution, scalability, and non-contact approach [11-14]. IJP consists of two techniques which include continuous inkjet and drop-on-demand inkjet [15-17]. In continuous inkjet technique, drops are produced continuously, and their paths are varied by the amount of charge applied. In drop-on-demand ink-jet technique, droplets are produced as needed (on demand) by applying the voltage only when a drop is desired. In the IJP process the liquid material is jetted out from the printer head (carrying an ink-filled cartridge) in a sequence of micro-droplets via a micrometer-sized nozzle head which are then solidified on the substrate. The deposited materials are in the form of chemical solutions and colloidal dispersions. The major actuation mechanisms of the inkjet nozzle head include thermal, piezoelectric and electrohydrodynamic. The benefits of IJP are compatibility with elastomers, mask less, reduced manufacturing costs, and the fabrication steps. The crucial challenges of the inkjet 3D printing technology in real-life applications are the need for inspection techniques and robust procedure to quantify and validate the process repeatability and component reproducibility. The significant requirements for any printing process include high throughput and high precision. An *in-situ* inspection tool is critical for IJP as minor drifts in process conditions can lead to large variations on the output part quality. To ensure the high throughput of the IJP process, *in-situ* monitoring and verification of the process parameters at each printing step is needed. There are numerous available sensing platforms, but they lack the high precision and throughput requirements and are quite expensive [18].

Vision-based approaches for *in-situ* quality assurance of AM processes can be employed for the enhancement of AM printing quality. Sensing, imaging and video devices such as cameras, sensors, and related devices are prominent for the implementation of *in-situ* process monitoring [19,20]. An efficacious real-time monitoring system plays a crucial role in quality assurance of the 3D printing process. The reliable monitoring system enables closed-loop control-based autonomous 3D printing systems along with the in-process diagnosis for AM processes. Over the past decades, numerous research studies have been conducted to establish advanced sensing technologies for the *in-situ* sensing and vision monitoring of 3D printing processes. Tapia and Elwany [21] reported a broad and thorough review of research efforts performed in the field of process monitoring and control for the improvement of part quality in metal-based AM process. Spears and Gold [22] conducted a progress review of process monitoring technology within the domain of Selective Laser Melting (SLM) additive manufacturing to establish a real-time quality assurance, and closed-loop feedback control of the SLM additive machine. Everton *et al.* [20] reported a state-of-the-art comprehensive review of various *in-situ* inspection and closed-loop control techniques employed in the assessment of AM printing quality. They reviewed literature that utilized pyrometry, the use of infrared cameras, visual and other camera/video-based methods for *in-situ* process monitoring. Qin *et al*. [23] demonstrated a real-time imaging characterization technique to create a real-time monitor system for printing detection. Their research also provided a foundation for an automated fabrication approach for E-jet printing. Other methods such as thermal imaging [24], high speed imaging [25], acoustic sensing, and inline coherent imaging [26] have been proposed as alternatives for *in-situ* monitoring of AM processes. Artificial intelligence (AI) and machine learning (ML) approaches were also utilized by researchers for process monitoring of different AM techniques. A comprehensive review of various artificial intelligence methods employed throughout AM are presented in [27] and [28]. A machine learning approach was utilized by Caggiano *et al.* [29] to develop on-line fault recognition through the use of automatic image processing in timely identifying material defects which occur as a result of process non-conformities in SLM of metal powders. Their research entailed the retrieval of in-process images captured during the layer-by-layer SLM process. These images were then examined via a bi-stream Deep Convolutional Neural Network-based model, and the recognition of SLM defective condition-related pattern was accomplished by automated image feature learning and feature fusion. Wu and Xu [30] utilized predictive models for predicting droplet velocity and volume using ensemble learning. Lin *et al.* [31] evaluated the two aspects of droplets profiles; droplet shape and temperature, using radial basis function neural networks. Huan *et al*. illustrated a deep learning method for unsupervised learning of droplet flow patterns. A deep recurrent neural network (DRNN) was used to execute the unsupervised learning portion of their research.

This research work focuses on the IJP process. Within this area, particular attention was devoted to *in-situ* monitoring of droplet formation since it poses one of the most vital components related to the quality and reliability of the IJP process. Ink droplet properties such as velocity, size, aspect ratio, and presence of satellites, are among the critical factors associated with droplet formation and behavior. Therefore, a crucial understanding of these parameters was investigated to create parts with geometric and operational integrity [32]. The main contributions of this paper include: 1) To apply a vision-based approach for *in-situ* monitoring of droplet formation. 2) Utilize machine learning models in studying the relationship between droplet parameters and droplet modes.

2. System overview

The FUJIFILM Dimatix material printer DMP 2850 with piezoelectric jetting system was employed in this research work. It has a resolution of 5 µm and repeatability of ±25 µm as shown in Fig. 1. The cartridge consists of a jetting module with 16 piezoelectric jetting nozzles, and a fluid module with a built-in fluid bag. The mechanism of an individual piezoelectric inkjet print nozzle is shown in Fig. 2. The nozzles can deliver a drop volume of 1 pL and 10 pL. For this research work, Dimatix fluid material was used for jetting the droplets for *in-situ* monitoring of the inkjet process. Drop watcher camera system was used to monitor the jetting behavior of each nozzle on-the-fly by modifying the waveform, voltage, and frequency setting.

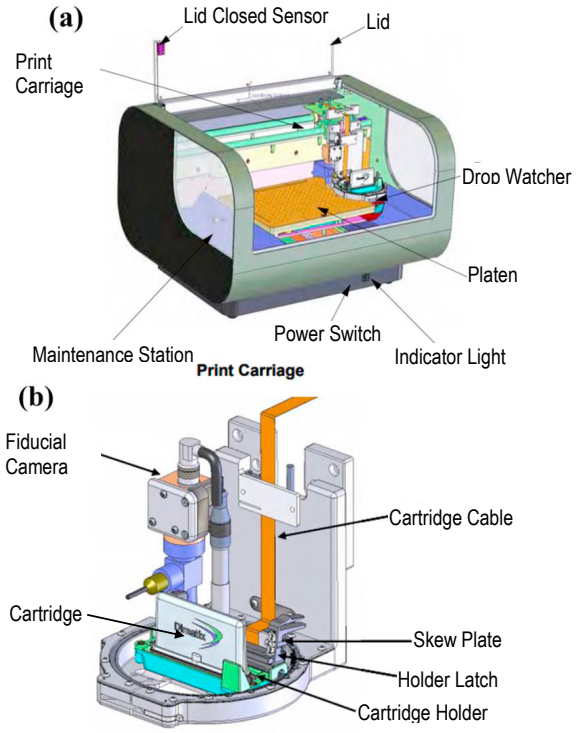

Fig. 1. (a) Dimatix-2850 inkjet printer; (b) printer cartridge assembly [33].

3. Methodology

The methodology was performed as two tasks which include (1) image acquisition and processing and (2) droplet classification using a neural network algorithm. For the real-time monitoring of inkjet printing, the following subtasks were performed:

1. Construction of matrix for equipment parameter settings;
2. Capturing of data;
3. Preprocessing of captured data;
4. Measuring of attributes of droplets from captured data;
5. Classification of droplets;
6. Training of machine learning algorithm;
7. Testing and validating of machine learning algorithm.

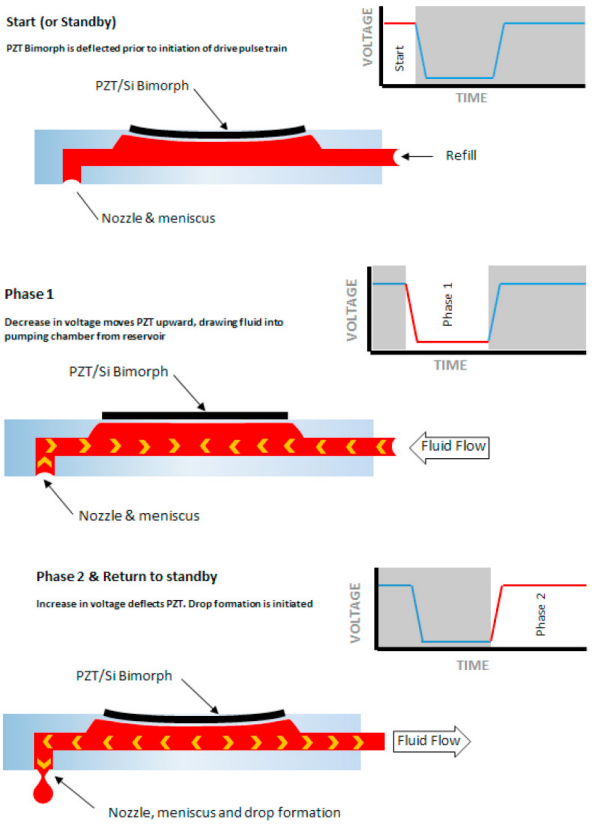

Fig. 2. Schematic diagram of a piezoelectric inkjet nozzle mechanism [33].

3.1. Construction of matrix for obtaining multiple droplet videos for feature extraction

The parameters of the DMP-2850 that were tuned for jetting the droplets were voltage and frequency. To capture different inkjet 3D printing scenarios, multiple videos at different voltage and frequency but at a constant waveform was recorded according to the constructed matrix in Table 1.

Table 1. Possible combinations of levels for voltage and frequency.

Sequence No.	Voltage (V)	Frequency (kHz)
1	15	5.6
2	25	5.6
3	30	5.6
4	15	7
5	25	7
6	30	7

3.2. Capturing of data

The drop watcher camera of the DMP-2850 was used to capture movies for a constant waveform and by setting frequency and voltage according to each experimental combination set as given in Table 1. For each movie, out of the sixteen piezoelectric jetting nozzles only a maximum of seven were activated to fit the camera view and reduce the volume

and size of data generated. The drop watcher generates 15 frames in a second and has a resolution of 720 pixels by 480 pixels by 3 channels.

3.3. Preprocessing of captured data

The videos obtained from the drop watcher camera contain noises which are from various sources. Some of those noises are from the cleaning mechanism during cleaning procedures of spitting, purging or blotting are carried out. Sometimes, ink droplets from nozzles that do not fire well could result in a bigger clogging of ink or splashes. As a result, we do not want to confuse a satellite for a noise in the system. Thus, one of the reasons we performed data preprocessing before analyzing, extracting, and measuring some droplet attributes. So, the concept of background subtraction was deployed to obtain our foreground (that is, ink droplets from each nozzle). To be consistent, a unique background frame was used for each movie as obtained according to session 3.2. The background frame was manually selected from the movie with the aid of a custom-written Python code and chiefly using OpenCV and NumPy libraries. A good background should have minimum or no noise and no initial ink droplet to provide only the region of interest when background subtraction is performed.

Our background subtraction was based on the principle of matrix addition and subtraction, for frames in the video, the foreground frames were obtained by subtracting the background frame from the considered frames. Mathematically, Equation 1 shows the relationship:

$$Fgd\_frame_i = frame_i - Bgd\_frame \quad (1)$$

where *Bgd_frame* is the background frame, Fgd_frame_i is the frame showing the considered ink droplet of the *i*th frame $frame_i$ is *i*th frame in the movie

After background subtraction, to have a better and clearer foreground frame that will aid analysis, further preprocessing was carried out using OpenCV functions (blur, thresh, and dilate).

3.4. Measuring attributes of droplets from captured data

After removing the noises from the images in each frame, we proceeded into capturing four main droplet attributes which include droplet size, aspect ratio, droplet velocity, and presence of satellites. For clarity, our chosen droplet parameters are described and explained as given below and illustrated in Fig. 3:

Droplet size: Droplet size is captured in this work with the droplet area. Minimum droplet size was set to 10 pixels to capture satellites if any.

Aspect ratio (AR): It is the ratio of droplet width to its height as *AR* = width/height. Four categories are used for our *AR,* round when *AR* is approximately 1, mid elongation when *AR* is greater than 0.5, high elongation when *AR* is less than 0.5, and none when *AR* is 0.

Droplet velocity: In this work, velocity is captured by measuring the distance of a droplet between two successive frames and the dividing by the time between the two frames. The video play rate is 15 fps (frames per second), and it is not the actual camera shutter speed. The camera of the Dimatix does not support kHz image capturing. The Dimatix software actually combines the images of different droplets under the same parameter settings and uses 15 fps (1s) in the video to depict the life of a droplet. As a result, the actual time between two consecutive frames will be 1/(Voltage frequency*15) seconds. The distance of the droplet movement during this time can be measured in pixels as shown in Fig. 3(c). This time and distance information can then yield the droplet velocity.

Satellite droplets: In this case, we are only interested to see if there are any lingering droplets after the main droplet. One of the properties assigned to satellites in this work is its area which is much smaller than its main droplet. With this, we can measure if there is a satellite or no-satellite.

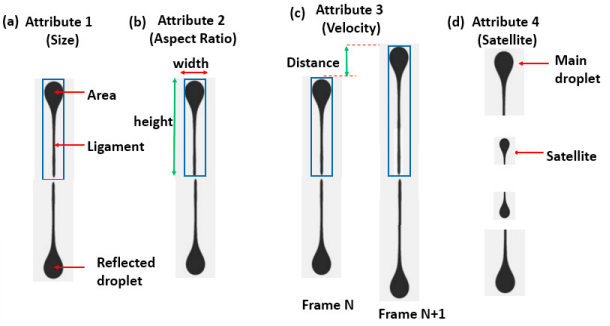

Fig. 3. (a) The droplet size is captured by the area of the droplet within the bounding box. The droplet below the bounding box is a mirrored or reflected droplet which they both have the same characteristics; (b) The dimension in red gives the width and green gives the height which are both used to calculate aspect ratio; (c) Two consecutive frames with the vertical distance between them are used for velocity calculation; (d) A main droplet and a satellite.

3.5. Classification of droplets

One of our tasks is to monitor the process in real-time. From the droplet attributes in session 3.4, each droplet from a nozzle in a frame is labelled according to its class. This led to supervised learning. In this work, three droplet modes were considered, these include normal, no-droplet, and satellite modes. In a piezoelectric actuator as in our printer case, frequency and voltage amplitude are some of the parameters that determine the type and nature of droplet formed as clearly explained in the works of [18] and [34].

Normal Droplet Mode: This is the desirable condition when a nozzle of the inkjet printer releases a fine drop of ink with consistent and uniform droplet size, having speeds and aspect ratios within + or - a given range, and with no satellites. Normal ink droplet is expected at a minimum voltage and frequency for the actuator to release fine ink droplet.

No-Droplet Mode: In this mode, one or more nozzles are not injecting out ink or the droplet details are not captured. So, droplet dimensions are not available. This could be because of insufficient voltage or frequency to cause a droplet release from the reservoir or one or more nozzles are clogged or not functional. This will result in voids in the printed parts.

Satellite Mode: This is a condition when there is at least one satellite droplet from a nozzle. Satellite droplet is an elongated part of the main droplet that are formed by a thread-like ink which are usually much smaller than the main droplet in size. This is usually caused by low ink particle concentrations or local trapping of particles despite having minimum voltage and frequency. The satellite droplets are usually not desirable as they will reduce the printing resolution.

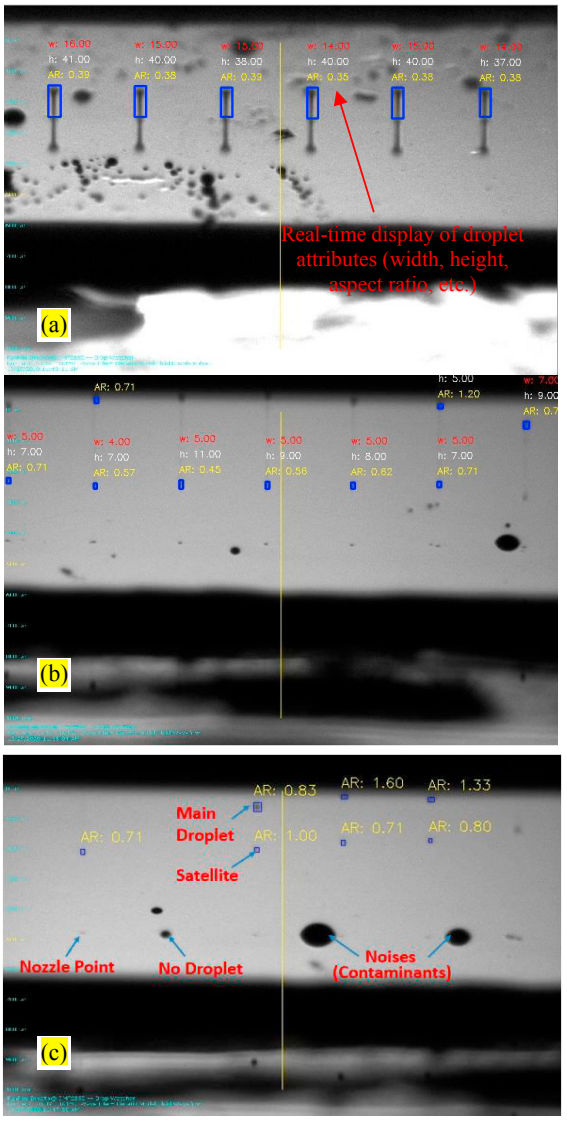

Fig. 4. (a) Normal droplet mode with width, height, and aspect ratio for six nozzles, (b) satellite droplet mode, and (c) satellite droplet mode with other features such as main droplets, satellites and nozzle point, no-droplet mode (blocked nozzle), and noises.

After data preprocessing, four nominal input features with their respective coded values were generated. From the code run on different movies as performed on each experiment, data were collected and presented in Table 2 to train and test the chosen machine learning algorithm. Fig. 4(a) and 4(b) show normal and satellite droplet modes displaying droplet width, height, and aspect ratio for all six nozzles activated with main droplets depicted above and mirrored droplets below for each nozzle point. Fig. 4(c) shows a view where satellite mode and no-droplet mode coexist for different nozzles. Raw datasets for different droplet attributes were extracted using the above-developed code. To capture reality, some of the noises are shown as depicted in Fig. 4(a), 4(b), and 4(c). It is worth to note that, these noises are contaminants caused during the inkjet 3D printer self-cleaning process.

Table 2. Input features and associated coded values.

Aspect Ratio (Code 1)	Size (Code 2)	Velocity (Code 3)	Satellite (Code 4)	Class
Round (1)	Normal (1)	Normal (1)	No (1)	Normal (1)
Mid-elongation (2)	Low (2)	Low (2)	One (2)	Satellite (2)
High-elongation (3)	High (3)	High (3)	Two or more (3)	No-droplet (3)
None (4)	None (4)	None (4)	N/A	N/A

3.6. BPNN-based machine learning for IJP process monitoring

The tradeoff between functionality and simplicity weighed heavily in the selection of the BPNN as the choice for the neural network algorithm. The BPNN was selected for use due to its; quick and easy implementation and being less complicated than other neural networks. In addition, the literature reveals that BPNN has previously been applied to the inkjet printing process [32,35]. A back propagation artificial neural network was developed to serve as a predictive model for different IJP droplet patterns. Typically, a normal droplet pattern is preferred in the IJP printing process, however, complications arise from determining the features or properties which influence droplet patterns. Therefore, the goal of the neural network model is to collect various droplet properties and assess the combination which gives a particular droplet mode. Neural network was employed to demonstrate the relationship between droplet properties and patterns. Back propagation neural network (BPNN) algorithm was used based on its high accuracy for predictive and classification purposes. The BPNN structure is made up of three layers: input layer, the hidden layer, and output layer. Its operation entails the computation of difference in error between the network's output and desired output which is then propagated back through the network. Error minimization is performed during the back-propagation process and involves the recurrent adjustment of weights within the network's intermediary layers. The required number of hidden units and layers are dependent on problem complexity.

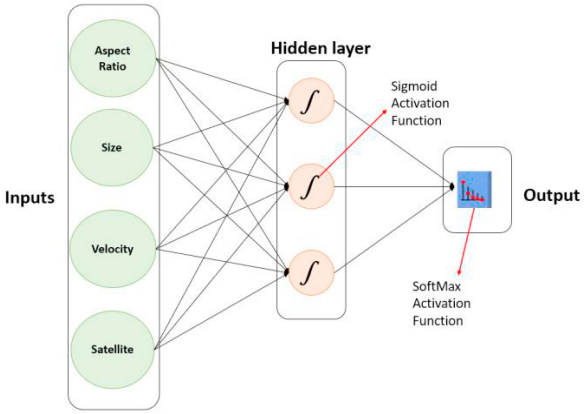

Fig. 5. The BPNN neural diagram.

For this research, a sigmoid and SoftMax activation function were used in the hidden and output layer, respectively, as shown in Fig. 5. The BPNN was constructed with four (4) input features: satellite droplets, droplet aspect ratio, droplet size, and droplet velocity and three (3) output patterns: normal, satellite, and no-droplet. As suggested by Chattopadhyay [36], and based on a sensitivity analysis for the number of hidden nodes, n=3 hidden nodes were used as this number gave the optimal tuning without overfitting the dataset. Source code in MATLAB R2017a was used to develop the BPNN model and evaluate its performance. The Levenberg-Marquardt (LM) algorithm was used to train the neural network. 95 sets of data were collected from some selected frames in different cycles associated with different video movies based on the three droplet modes to train and test the neural network model. The data consisted of input features and output patterns which were assigned numerical nomenclature (code) as seen in Table 3, and split into two sets: the training dataset, comprising of about 70% of the entire dataset and test dataset containing the remaining 30%.

Table 3. Snapshot of dataset.

Data Index	Aspect Ratio	Size	Velocity	Satellite	Class Output
1	1	1	1	1	1
2	4	4	4	1	3
3	3	1	2	2	2
4	2	2	2	3	2
5	3	2	3	3	2
6	2	2	1	2	2
7	3	2	1	3	2
8	1	1	1	2	2

To address the initial paucity of training data, k - fold cross-validation method [37] was used. The dataset was randomly split into k equal-size subsamples. The k-1 subsamples were used as a training dataset and the leftover single subsample was used for validating the model. The cross-validation process was then repeated for k times, with each of the k subsamples used exactly once as the validation data. A 4-fold cross-validation was performed, which enabled the algorithm to evaluate 4 folders (each group holds 25% of the training dataset to be tested 4 times) in random to conduct the analysis. Thus, the total datasets for the algorithm were augmented to N = 380 data points. Each fold was also applied to prevent the overfitting of the problem. For testing, 30% of the entire dataset was used to test the accuracy of the BPNN models.

4. Results and Discussion

The prediction performance of the BPNN was assessed based on the accurate classification of the test data set. A confusion matrix was applied to detect the prediction accuracy of the network. Fig. 6. illustrates the confusion matrix for the BPNN which had an overall accuracy of 90%. The nomenclature droplet patterns in the confusion matrix are as follows: Normal: 1, Satellite: 2 and No-droplet: 3. Out of the 30 test data, 3 were classified incorrectly and the remaining 27 were classified correctly. In addition to the confusion matrix, the target output from test data was plotted against the network output to demonstrate the efficacy of the network as seen in Fig. 7. Overall, considering the limited data, the BPNN gave highly accurate results and demonstrated the efficacy of neural network application on *in-situ* droplet monitoring. It is believed that the accuracy can be higher with more available data.

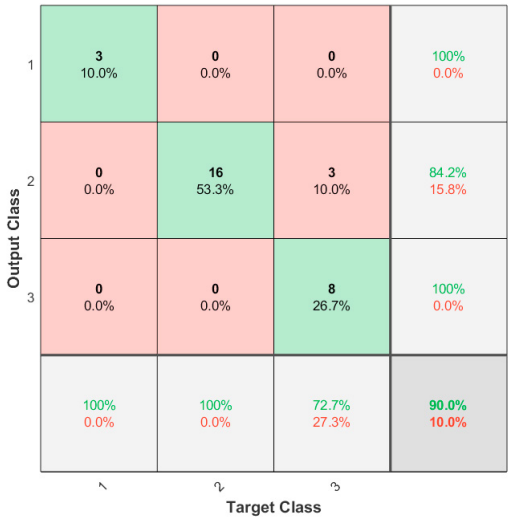

Fig. 6. BPNN Confusion Matrix.

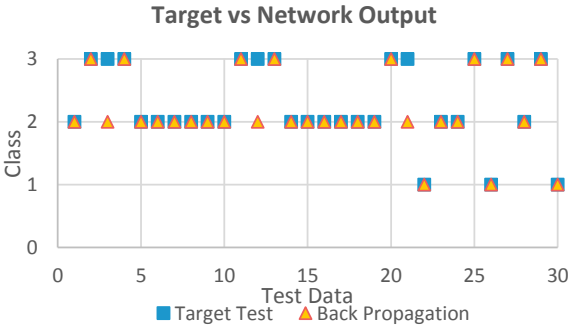

Fig. 7. Target Output vs BPNN Output.

5. Conclusion and Future Work

In this research work, we demonstrated a novel *in-situ* process monitoring for inkjet-based 3D printing systems. The framework utilized in this paper integrates the image processing technique and machine learning algorithms for vision-based approach of *in-situ* monitoring of droplet formation. A sequence of videos was captured by a drop watcher camera for different voltage and frequency combinations. The four attributes (droplet size, aspect ratio, droplet velocity, presence of satellites) of the droplet were extracted from the video frames to categorize the behavior of the droplet (normal, no-droplet, and satellite modes). A backpropagation artificial neural network (BPNN) was developed to integrate various droplet properties and assess the combination which gives a particular droplet mode. The overall accuracy of the BPNN for classification of the test data set was around 90% and thus illustrates the efficacy of neural network application for *in-situ* droplet monitoring.

This paper presents our ongoing work, which is a preliminary part of our long-term goal of a digital twin model of inkjet 3D printing towards process optimization and closed-loop control. The feasible, simplicity and accuracy of the BPNN method presented in the paper provides the foundation for our future advancement. Based on the identification of the current droplet mode, a closed-loop control method will be developed in the future by adjusting the key control parameters (e.g., voltage and frequency) and keeping the droplets in the desirable mode.

Acknowledgements

The authors would like to express their gratitude for funding support from the National Science Foundation Grant (NSF CMMI Award #1663128) and the Center of Excellence in Product Design and Advanced Manufacturing at North Carolina A&T State University.

References

[1] Tofail SA, Koumoulos EP, Bandyopadhyay A, Bose S, O'Donoghue L and Charitidis C. Additive manufacturing: scientific and technological challenges, market uptake and opportunities. Materials today, 2018; 21(1): 22-37.

[2] ASTM. Standard terminology for additive manufacturing technologies. ASTM International; 2012.

[3] Attaran M. The rise of 3-D printing: The advantages of additive manufacturing over traditional manufacturing. Business Horizons, 2017; 60(5): 677-688.

[4] Desai S and Haeberle G. Additive Manufacturing (3D Printing) of Thermoform Tooling. International Journal of Mechanical and Production Engineering, 2019; 7(3): 1-4.

[5] Aldawood FK, Chang SX and Desai S. Design and manufacture of a high precision personalized electron bolus device for radiation therapy. Medical Devices & Sensors, e10077.

[6] Haeberle G and Desai S. Investigating Rapid Thermoform Tooling Via Additive Manufacturing (3d Printing). American Journal of Applied Sciences, 2019; 16238-243.

[7] Desai S, Craps M and Esho T. Direct writing of nanomaterials for flexible thin-film transistors (fTFTs). The International Journal of Advanced Manufacturing Technology, 2013; 64(1-4): 537-543.

[8] Aljohani A and Desai S. 3D printing of porous scaffolds for medical applications. American Journal of Engineering and Applied Sciences, 2018; 11(3).

[9] Parupelli SK and Desai S. A comprehensive review of additive manufacturing (3d printing): Processes, applications and future potential. American Journal of Engineering and Applied Science, 2019; 16244-272.

[10] Singh M, Haverinen HM, Dhagat P and Jabbour GE. Inkjet printing—process and its applications. Advanced materials, 2010; 22(6): 673-685.

[11] Parupelli SK and Desai S. Understanding hybrid additive manufacturing of functional devices. American Journal of Engineering and Applied Sciences, 2017; 10(1): 264-271.

[12] McKenzie J and Desai S. Investigating sintering mechanisms for additive manufacturing of conductive traces. American Journal of Engineering and Applied Sciences, 2018; 11(2).

[13] Parupelli SK and Desai S. Hybrid additive manufacturing (3D printing) and characterization of functionally gradient materials via in situ laser curing. The International Journal of Advanced Manufacturing Technology, 2020; 110(1): 543-556.

[14] Salim A and Lim S. Review of recent inkjet-printed capacitive tactile sensors. Sensors, 2017; 17(11): 2593.

[15] Desai S and Lovell M. Modeling fluid–structure interaction in a direct write manufacturing process. Journal of Materials Processing Technology, 2012; 212(10): 2031-2040.

[16] Desai S, Lovell M and Cordle J. Coupled field analysis of a piezoelectric bimorph disc in a direct write process. Composites Part B: Engineering, 2007; 38(7-8): 824-832.

[17] Desai S and Lovell M. Computational fluid dynamics analysis of a direct write manufacturing process. International Journal of Nanomanufacturing, 2009; 3(3): 171-188.

[18] Guo Y, Patanwala HS, Bognet B and Ma AW. Inkjet and inkjet-based 3D printing: connecting fluid properties and printing performance. Rapid Prototyping Journal, 2017.

[19] Grasso M and Colosimo BM. Process defects and in situ monitoring methods in metal powder bed fusion: a review. Measurement Science and Technology, 2017; 28(4): 044005.

[20] Everton SK, Hirsch M, Stravroulakis P, Leach RK and Clare AT. Review of in-situ process monitoring and in-situ metrology for metal additive manufacturing. Materials & Design, 2016; 95431-445.

[21] Tapia G and Elwany A. A review on process monitoring and control in metal-based additive manufacturing. Journal of Manufacturing Science and Engineering, 2014; 136(6).

[22] Spears TG and Gold SA. In-process sensing in selective laser melting (SLM) additive manufacturing. Integrating Materials and Manufacturing Innovation, 2016; 5(1): 16-40.

[23] Qin H, Zhang X, Singh R, Zhang Z and Chen Y. In-process monitoring of electrohydrodynamic inkjet printing using machine vision. In Proceedings of AIP Conference Proceedings, 2102, 2019, 070008.

[24] Lane B, Moylan S, Whitenton EP and Ma L. Thermographic measurements of the commercial laser powder bed fusion process at NIST. Rapid Prototyping Journal, 2016.

[25] Bertoli US, Guss G, Wu S, Matthews MJ and Schoenung JM. In-situ characterization of laser-powder interaction and cooling rates through high-speed imaging of powder bed fusion additive manufacturing. Materials & Design, 2017; 135385-396.

[26] Kanko JA, Sibley AP and Fraser JM. In situ morphology-based defect detection of selective laser melting through inline coherent imaging. Journal of Materials Processing Technology, 2016; 231488-500.

[27] Yang J, Chen Y, Huang W and Li Y. Survey on artificial intelligence for additive manufacturing. In Proceedings of 2017 23rd International Conference on Automation and Computing (ICAC), 2017, 1-6.

[28] Razvi SS, Feng S, Narayanan A, Lee Y-TT and Witherell P. A review of machine learning applications in additive manufacturing. In Proceedings of ASME 2019 International Design Engineering Technical Conferences and Computers and Information in Engineering Conference, 2019,

[29] Caggiano A, Zhang J, Alfieri V, Caiazzo F, Gao R and Teti R. Machine learning-based image processing for on-line defect recognition in additive manufacturing. CIRP Annals, 2019; 68(1): 451-454.

[30] Wu D and Xu C. Predictive modeling of droplet formation processes in inkjet-based bioprinting. Journal of Manufacturing Science and Engineering, 2018; 140(10).

[31] Lin X, Zhu K, Zhou J and Fuh JYH. Intelligent modeling and monitoring of micro-droplet profiles in 3D printing. ISA Transactions, 2020.
[32] Wang T, Kwok T-H, Zhou C and Vader S. In-situ droplet inspection and closed-loop control system using machine learning for liquid metal jet printing. Journal of manufacturing systems, 2018; 4783-92.
[33] Fujifilm. Dimatix Materials Printer DMP-2850 User Manual. Fujifilm; 2019.
[34] Reis N, Ainsley C and Derby B. Ink-jet delivery of particle suspensions by piezoelectric droplet ejectors. Journal of Applied Physics, 2005; 97(9): 094903.
[35] Ball AK, Das R, Roy SS, Kisku DR and Murmu NC. Modeling of EHD inkjet printing performance using soft computing-based approaches. Soft Computing, 2020; 24(1): 571-589.
[36] Chattopadhyay R 2011. Artificial neural networks in yarn property modeling. Soft Computing in Textile Engineering. Elsevier.
[37] Wong T-T and Yang N-Y. Dependency analysis of accuracy estimates in k-fold cross validation. IEEE Transactions on Knowledge and Data Engineering, 2017; 29(11): 2417-2427.